

4 RESULTS AND DISCUSSION

4.1 *In silico* analysis of RsaF – a small non-coding RNA of *Staphylococcus aureus*

The sRNA RsaF identified in *S. aureus* is conserved among other staphylococcal strains (N315, RN6390, COL, Newman) (Geissmann *et al.* 2010). RsaF, a 104bp long sRNA flanked by two hypothetical proteins was predicted to have a secondary structure with three stem loops (Figure 10).

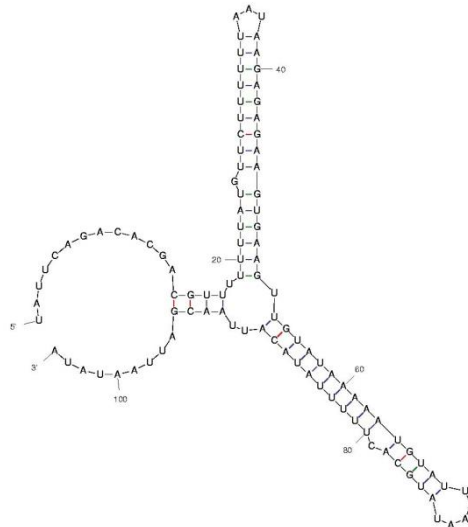


Figure 10: Secondary structure of RsaF predicted by S-fold.

RsaF was analyzed by bioinformatics using software Target RNA, TargetRNA2, IntaRNA, and CopraRNA, belonging to two different categories (Pain *et al.*, 2015), to screen for candidate virulence genes as potential targets that are assayable physiologically. The Target RNA program belonging to the “inter-RNA” category (Pain *et al.*, 2015), that employs a nearest neighbor thermodynamic model restricted to interactions between sRNA and mRNA, ignoring intra molecular base-pairs, identified Hyaluronate lyase (*hysA*), a potent virulence and spreading factor of infection, as a potential virulent target. On the other hand, the programs belonging to the “independent fold” group (TargetRNA2, IntaRNA and CopraRNA), which analyze the secondary structure folding landscape, independently for each RNA, and computes the total binding energy as a sum of 2 contributions, listed Serine Protease Like protein (*spID*) as a target. A comparative list of putative targets of RsaF predicted by different programs is listed in the Table 14.

Table 14: Target predicted for sRNA RsaF by various programs.

	TargtRNA		TargetRNA2		CoprRNA		RNA predator	
Rank	Name	Pvalue	Name	Pvalue	Name	p-value	Name	Z-score
1	hypothetical protein	0.000433	serine protease SplD	0	50S ribosomal protein L20	6.87E-05	leucyl tRNA synthetase NWMN	-4.6
2	PTS system, mannitol specific IIBC component	0.000433	secretory antigen SsaA-like protein	0.004	50S ribosomal protein L10	0.000394	hypothetical protein NWMN 2113 NWMN	-3.89
3	hypothetical protein	0.000743	hypothetical protein	0.008	1,4-dihydroxy-2-naphthoate polyprenyltransferase	0.000401	phosphoenolpyruvate protein phosphatase NWMN	-3.88
4	hypothetical protein	0.001273	ribosome biogenesis GTP-binding protein YsxC	0.01	serine protease SplD	0.000481	serine protease SplD NWMN	-3.71
5	serine protease SplB	0.001523	universal stress protein family protein	0.022	Derived by automated computational analysis using gene prediction method: Protein Homology.	0.000603	1;4 dihydroxy 2 naphthoate octaprenyltransferase NWMN	-3.59
6	superantigen like protein	0.002609	phosphocarrier protein HPr	0.03	phenol-soluble modulins export ABC transporter permease subunit PmtB	0.000609	ABC transporter; ATP binding MsbA family protein NWMN	-3.59
7	hypothetical protein	0.003735	cation efflux family protein	0.03	4-hydroxy-tetrahydrodipicolinate reductase	0.001495	hypothetical protein NWMN 1011 NWMN	-3.45
8	hypothetical protein	0.003735	acetyltransferase, GNAT	0.034	elongation factor Ts	0.001835	hypothetical protein NWMN	-3.45

			family protein				0283 NWMN	
9	hypothetical protein	0.003735	hypothetical protein	0.034	catabolite control protein A	0.001853	hypothetical protein NWMN 1797 NWMN	-3.45
10	hyaluronate lyase precursor	0.005346	hypothetical protein	0.036	anti-sigma B factor RsbW	0.001898	sensor kinase protein NWMN	-3.36
11	hypothetical protein	0.005346	hypothetical protein	0.037	GTP-binding protein	0.001983	hypothetical protein NWMN 0347 NWMN	-3.27
12	preprotein translocase subunit SecG	0.006394	hypothetical protein	0.038	type II pantothenate kinase	0.002251	elongation factor Ts NWMN	-3.23
13	hypothetical protein	0.006394	fructose 1-phosphate kinase	0.04	dihydrolipoamide dehydrogenase	0.002661	50S ribosomal protein L10 NWMN	-3.2
14	hypothetical protein	0.006394	hypothetical protein	0.042	DUF2187 domain-containing protein	0.003267	hypothetical protein NWMN 2542 NWMN	-3.17
15	hypothetical protein	0.006394	formyl peptide receptor-like inhibitory protein ¹	0.044	Derived by automated analysis using gene prediction method: Protein Homology.	0.507781	DNA binding response regulator NWMN	-2.94
16							Hyaluronate lyase precursor NWMN	0.08

Virulence factors hyaluronate lyase (HysA) and serine protease like protein D (SplD) have been selected as mRNA targets for sRNA RsaF. HysA is an extracellular enzyme capable of degrading hyaluronic acid (HA) present in the connective tissue. HA is a versatile component of many physiological processes including cell proliferation, adhesion and inflammation. Serine protease like protein D (SplD) encoded in an *spl* operon (a group of six serine proteases *splA-splF*) is known as inducer of allergic asthma.

4.2 Interaction of RsaF with selected putative mRNA targets

Both *hysA* and *spID* mRNA targets of RsaF displayed base pairing of 15 - 22nt with acceptable P values (≤ 0.01) by their respective programs. The interactions of these target mRNAs were further confirmed by IntaRNA. RsaF interacts at the 5' untranslated regions (UTRs) of *hysA* mRNA (-22 to +8) (Fig. 1A), and *spID* (-56 to -39) (Figure 11).

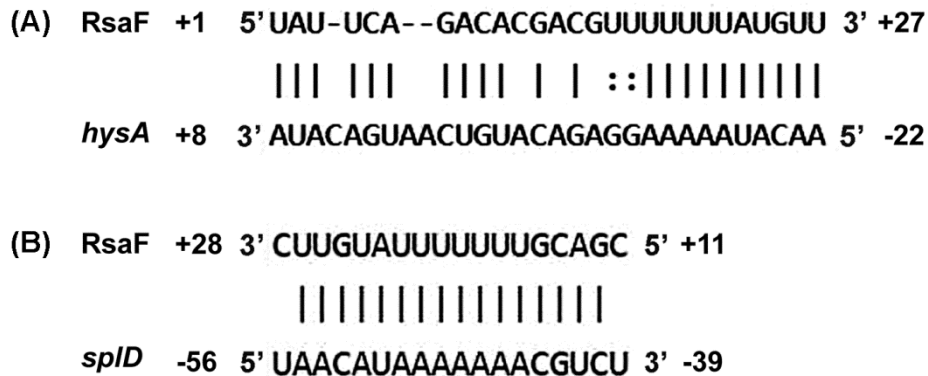


Figure 11: *In Silico* analysis of RsaF and its interaction with predicted targets by Target RNA program.

(A) RsaF-*hysA* mRNA interaction. (B) RsaF-*spID* mRNA base pairing.

4.3 Overexpression of RsaF from a multi-copy plasmid

rsaF gene was amplified from *S. aureus* genomic DNA with RsaFF/ RsaFR primers (Table 11) and a band of approximately 273 bp was obtained (Figure 12A) which was eluted and cloned in the vector pBluescript II KS(+) using XbaI and PstI sites. The clones were confirmed by restriction digestion with PvuII (Figure 12B) and further with DNA sequencing at MWG Eurofins Ltd., Bangaluru. RsaF fragment was released by PstI and XbaI digestions from pBluescript II KS (+) and sub-cloned in *Escherichia-Staphylococcus* shuttle vector pCN40 to generate pCN*rsaF*.

The clones were confirmed by insert release with EcoRI and HindIII (275 bp) (Figure 12C). The above constructs were made in *E. coli* DH5 α and were later passed through *S. aureus* RN4220 as an intermediate host to bypass the restriction barrier followed by electroporation into *S. aureus* Newman. The *S. aureus* clone plasmid, pCN*rsaF* was confirmed by restriction digestion with ClaI giving three bands of 2493 bp, 1871 bp and 1726 bp whereas digestion of control plasmid gives two bands of 4103bp and 1728bp (Figure 12D).

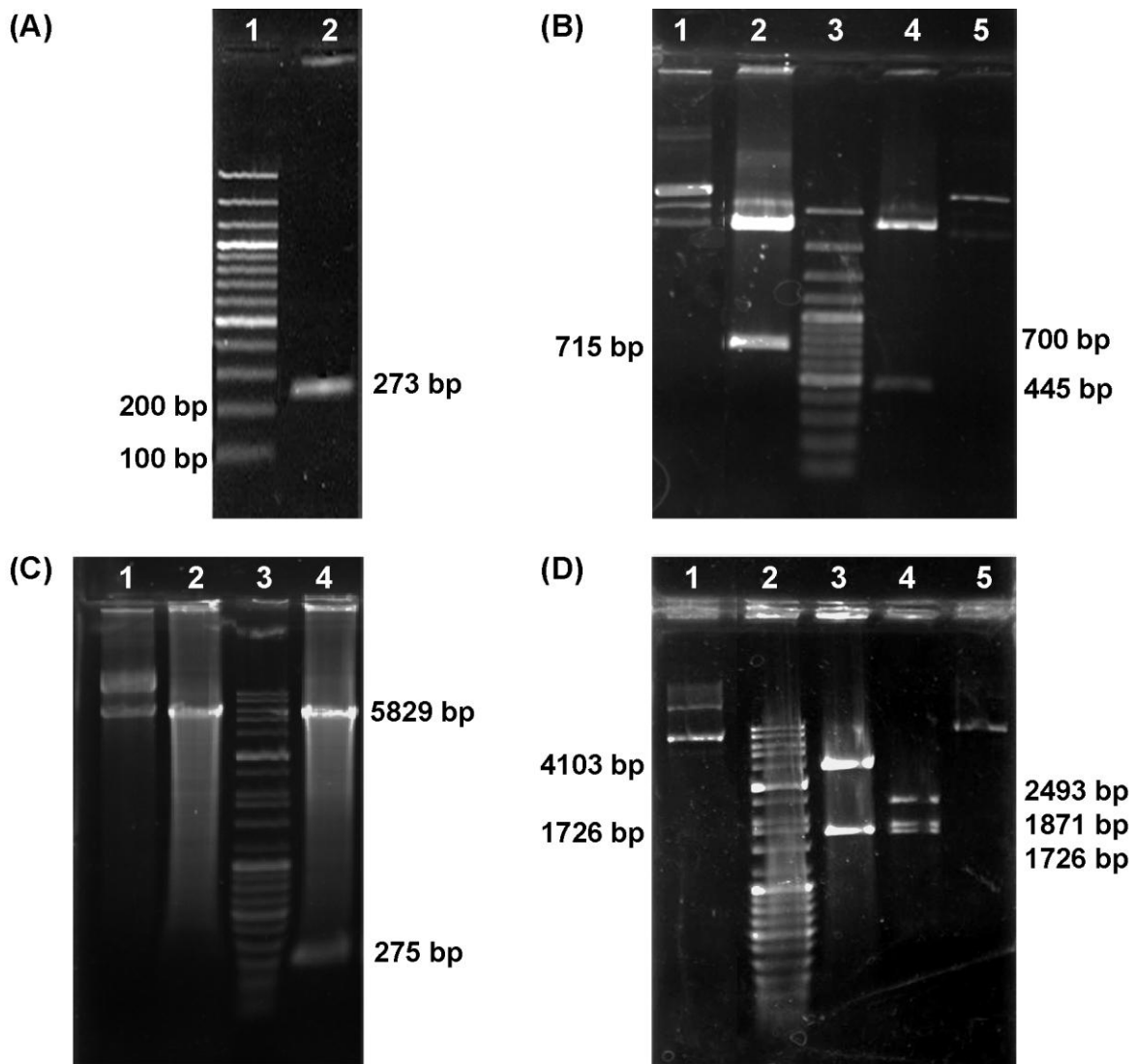


Figure 12: PCR amplification, cloning and sub-cloning of RsaF

(A) PCR amplification of *RsaF*. Lane 1: Medium range marker, Lane 2: *RsaF* (273bp). (B) Restriction digestion analysis of *pBSKsrsaF*; Lane 1: Undigested clone plasmid, Lane 2: Clone digested with *PvuII* (715bp), Lane 3: Medium range marker, Lane 4: *pBSKS* digested with *PvuII* (445 bp), Lane 6: undigested *pBSKS*. (C) *pCNrsaF* clone confirmation in *E. coli*. lane 1: Undigested *pCN40*, Lane 2: *BamHI* and *PstI* digested *pCN40* (5.8 kb), Lane 3: High range marker, Lane 4: *pCNRsaF* digested with *BamHI* and *PstI* (5.8 kb & 275 bp) (D) *pCNrsaF* clone confirmation in *S. aureus* Newman. Lane 1: Undigested *pCN40*, Lane 2: High range Marker, Lane 3: *ClaI* digested *pCN40* (4103bp & 1728bp), Lane 4: *ClaI* digested *pCNrsaF* (2493 bp, 1871 bp & 1726 bp), Lane 5: Undigested *pCNrsaF*.

4.4 Disruption of *RsaF* chromosomal copy with kanamycin resistance marker

A disruption mutant of *rsaF* in *S. aureus* Newman was generated by inserting a kanamycin resistance gene (Km) in *rsaF* by homologous recombination. A 3-step PCR protocol depicted in Figure 13 was used to generate the gene disruption cassette (GDC) of *rsaF* and was cloned in a TA vector (*pTZ57R/T*).

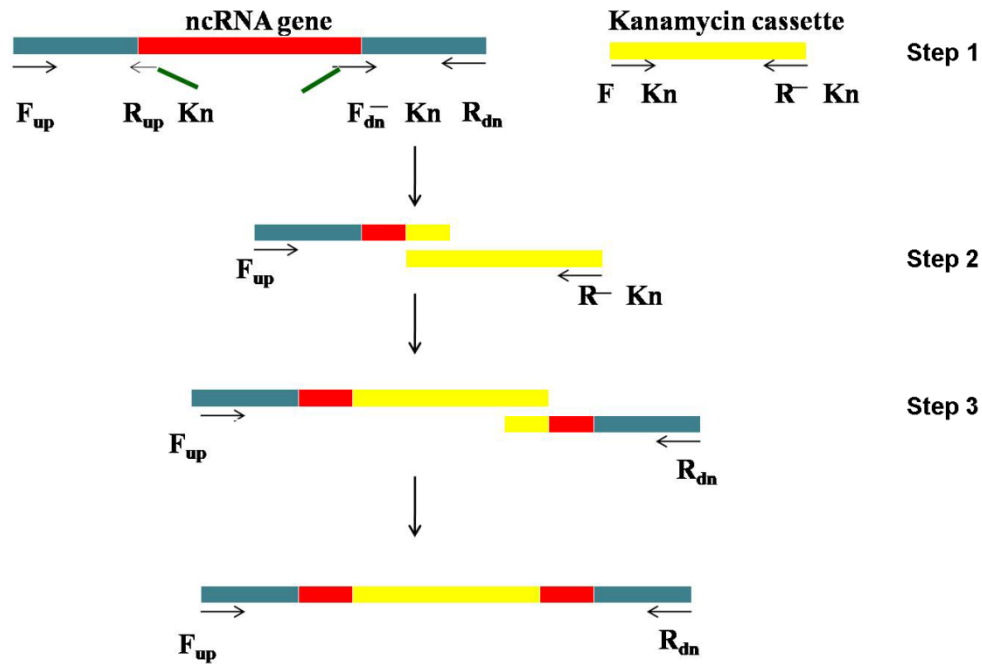


Figure 13: Pictorial representation of 3-step fusion PCR to generate gene disruption cassette

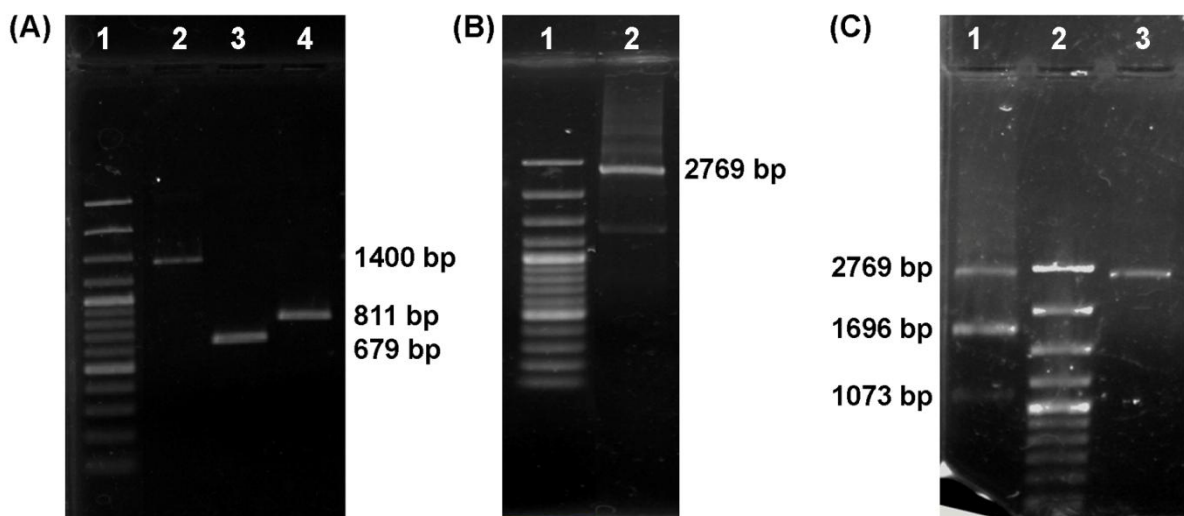


Figure 14: RsaF Gene disruption cassette construction and confirmation

(A) PCR amplifications for RsaF Gene disruption cassette; Lane 1: Marker, Lane 2: Kanamycin marker (1400bp), Lane 3: upstream flanking region of RsaF (679bp), Lane 4: downstream flanking region of RsaF gene (811bp). (B) Lane 1: Marker, Lane 2: Fusion PCR product of Kanamycin gene, upstream and downstream flanking region of RsaF gene (2769bp). (C) Confirmation of RsaFGDC; Lane 1: RsaFGDC digested with NsiI (1696bp & 1073bp), Lane 2: Marker, Lane 3: Undigested RsaFGDC (~2769bp).

Amplicons of the upstream and downstream regions of *rsaF*, 679 bp and 811 bp respectively containing the 5' and 3' end of the *rsaF* and 855 bp long kanamycin marker were obtained by PCR (Figure 14A). These amplicons were then joined together by an overlap extension PCR to obtain a 2769 bp long *rsaF* GDC (Figure 14B). The *rsaF* GDC thus obtained was gel

eluted and further confirmed by restriction digestion with NsiI, giving digested bands of 1696 bp and 1073 bp (Figure 14C).

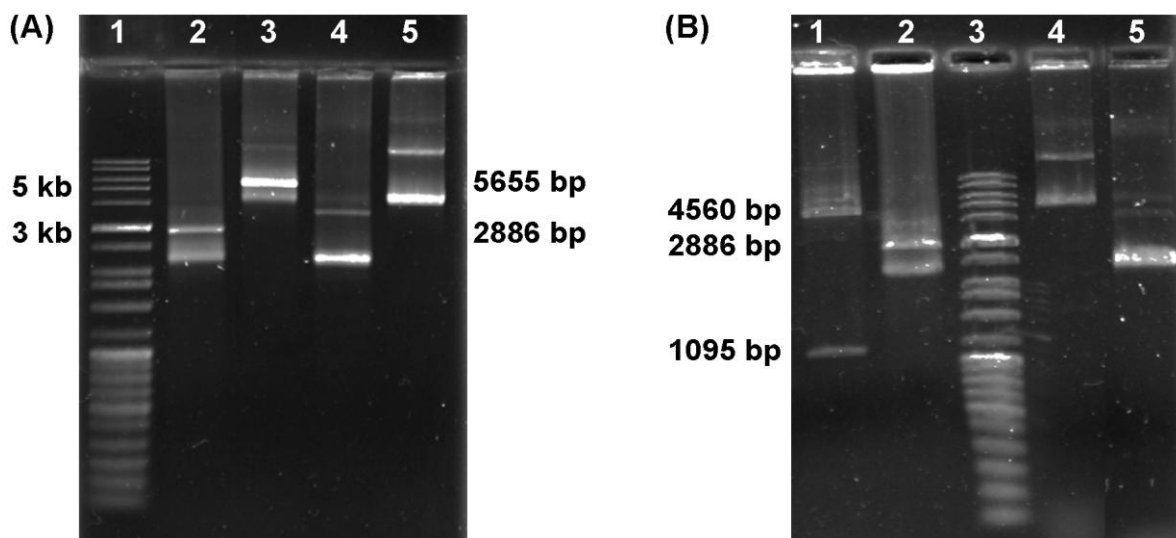


Figure 15: pTZRsaFGDC clone confirmation

(A) Linearization of clone plasmid. Lane 1: Marker Lane 2: KpnI digested pTZ57T/R, Lane 3: pTZRsaFGDC digested with KpnI, Lane 4: undigested pTZ57R/T, Lane 5: Undigested pTZRsaFGDC. (B) Insert cut of RsaFGDC with PstI Digestion. Lane 1: PstI digested pTZRsaFGDC, Lane 2: PstI digested pTZ57R/T, Lane 3: Marker, Lane 4: Undigested pTZRsaFGDC, Lane 5: Undigested pTZ57R/T.

RsaFGDC was ligated with plasmid pTZ57R/T with 3' dT overhangs as per the manufacturer's instructions (InsTAclone PCR Cloning Kit, Fermentas). The clones were confirmed by linearization with KpnI (Figure 15A) and insert cut using PstI (Figure 15B).

rsaFGDC was subcloned in temperature sensitive shuttle vector pMAD and clones were confirmed by insert release of 2.8 kb with BamHI and SalI (Figure 16A). pMAD*rsaFGDC* was electroporated into *S. aureus* Newman after passing through *E. coli* DC10B strain to create *rsaF::kan* mutants. Kanamycin resistant and erythromycin sensitive white colony that grew at 42°C resulting from a double cross over event and loss of the vector was selected and analyzed for *rsaF* chromosomal disruption by colony PCR with different pairs of primers (Figure 16B). The *rsaF* disruption mutant was also screened by an increase in 1.4 kb giving amplicon of 2.9 kb when amplified using flanking region primers and presence of 1.4 kb kanamycin gene by kanamycin specific primers (Figure 16B).

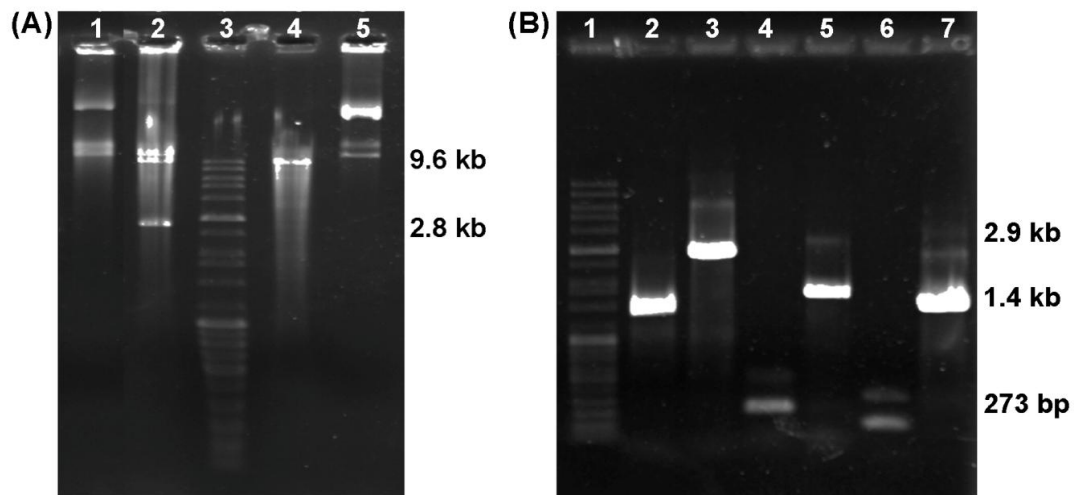


Figure 16: pMADRsaFGDC clone confirmation

(A) Insert release of pMADRsaFGDC in *E. coli*. Lane 1: Undigested pMADRsaFGDC, Lane 2: BamHI and Sall digested pMADRsaFGDC, Lane 3: Marker, Lane 4: pMAD digested with BamHI and Sall, Lane 5: Undigested pMAD. (B) Confirmation of disrupted RsaF in *S. aureus* Newman by colony PCR. Lane 1: Marker, Amplification with RsaF 5' and 3' flanking region primers, Lane 2: *S. aureus* Newman (1.5 kb), Lane 3: *rsaF::Kan* (2.9 kb). Amplification with RsaF ncRNA primers, Lane 4: *S. aureus* Newman (273 bp), Lane 5: *rsaF::Kan* (1.6 kb). Amplification with kanamycin primers, Lane 6: *S. aureus* Newman, Lane 7: *rsaF::Kan* (1.4 kb).

4.5 Confirmation of *rsaF* gene disruption in *S. aureus* Newman

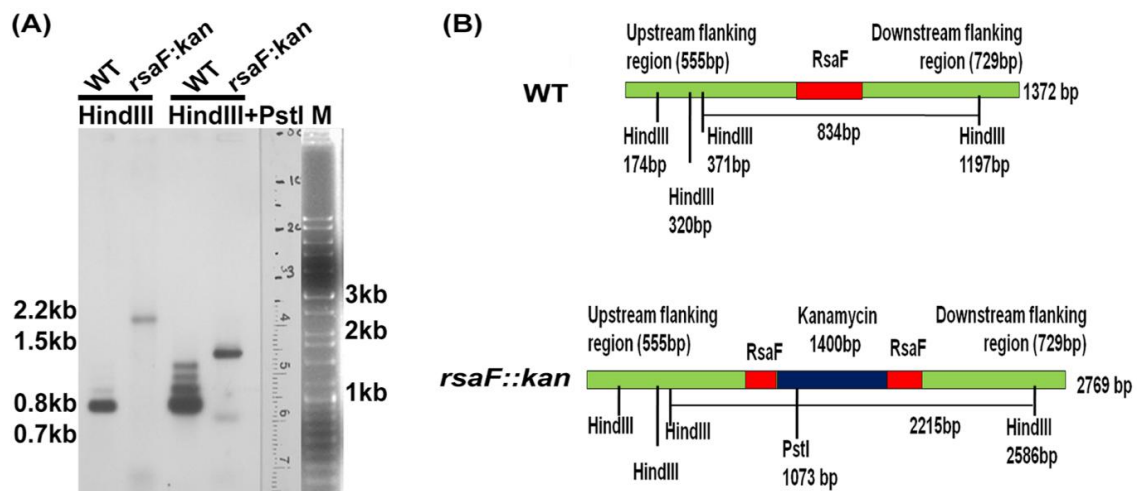


Figure 17: Confirmation of *rsaF* gene disruption in *S. aureus* Newman

(A) Southern blot analysis of *rsaF* disruption (*rsaF::kan*) and the wild type (WT) *S. aureus* Newman. M- Marker, 100 to 10000 bp. (B) Schematic representation of the genomic DNA of wild type and *rsaF* disruption strain digested with HindIII and PstI.

The chromosomal copy of *rsaF* gene was disrupted, by inserting a kanamycin marker by homologous recombination, using a temperature sensitive shuttle vector pMAD. The disruption of *rsaF* was confirmed by southern blot (Figure 17A). Genomic DNA was digested with HindIII and HindIII + PstI followed by hybridization with DIG-labeled RsaF

probe. The chromosomal disruption of *rsaF* was indicated by an increase of 1.4 kb in the molecular weight of bands 2.2 kb and 1.5 kb when digested with HindIII and HindIII + PstI respectively (Figure 17).

4.6 Expression analysis of RsaF in modified *S. aureus* strains

Analyses of expression of *rsaF* in pCN*rsaF* by northern blotting indicated transcript of 274 nt from PblaZ promoter. Strain bearing vector pCN40 served as the control. The 240 nt transcripts in both the control and overexpression strain are likely to be expressed from chromosomal copy (Figure 18A). The 273 nt transcript of RsaF expressed from PblaZ promoter in the overexpression strain was structurally similar to the chromosomal copy of 240 nt and was shown to base pair with the target transcripts at the same nucleotides as would the chromosomal RsaF, as analyzed by IntaRNA program.

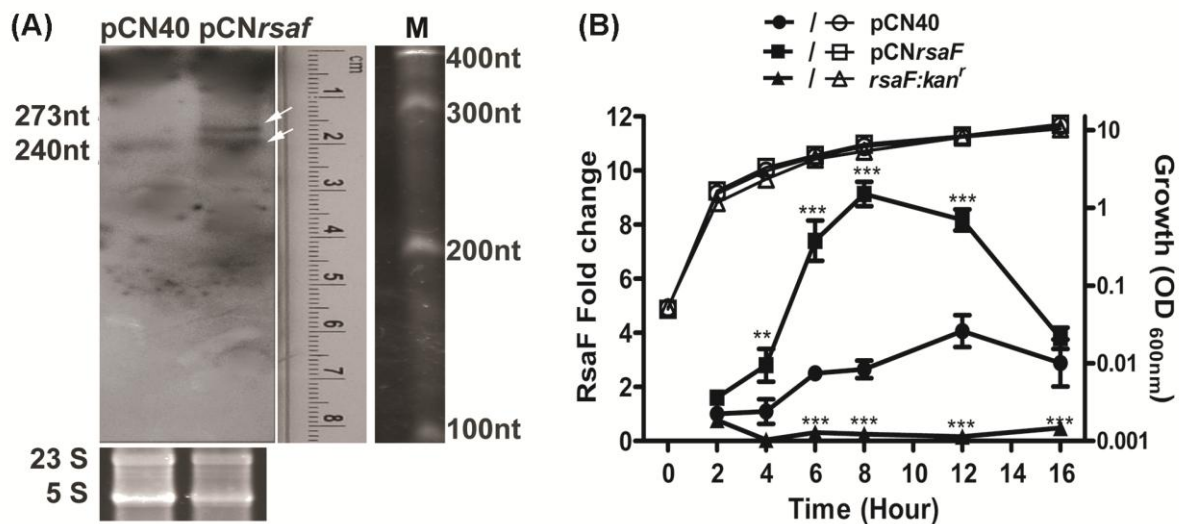


Figure 18: Expression analysis of RsaF overexpression by northern blotting.

(A) Northern blot hybridized with DIG-labeled RsaF probe, showing expression of chromosomal copy in control (pCN40) and additionally from plasmid in overexpression (pCN*rsaF*) strain. Ethidium bromide stained 23S and 16S rRNA bands on agarose gels are shown as RNA loading controls. (B). qRT-PCR of RsaF mRNA in overexpression (pCN*rsaF*), disruption (*rsaF::kan*) and control pCN40 strains along growth. Data normalized with 5S rRNA and 2h expression as the calibrator. Filled symbols (●/■/▲) indicate the fold change in RsaF expression and open symbols (○/□/△) indicate the growth. Fold change was calculated as per standard $\Delta\Delta C_t$ method. The experiment was performed in triplicates; mean and standard deviation are plotted. * represents the statically significant difference analyzed by two-way ANOVA. ***($P < 0.001$) and **($P < 0.01$).

Expression of altered levels of RsaF in modified strains was compared by qRT-PCR.

The levels of *rsaF* transcripts increased by 1.6–3.5 fold from early exponential phase to stationary phase in overexpression (pCN*rsaF*) strain in qRT-PCR (Figure 18B). The expression of *rsaF* was maximum at the transition of log to stationary phase of growth, as

compared to the control. qRT-PCR analysis of disruption strain showed a marked reduction of *rsaF* transcripts to 0.03 fold (Figure 18B).

4.7 Influence of altered RsaF levels on the expression of hyaluronate lyase (HysA)

4.7.1 RsaF positively influences the expression of HysA in *S. aureus* Newman

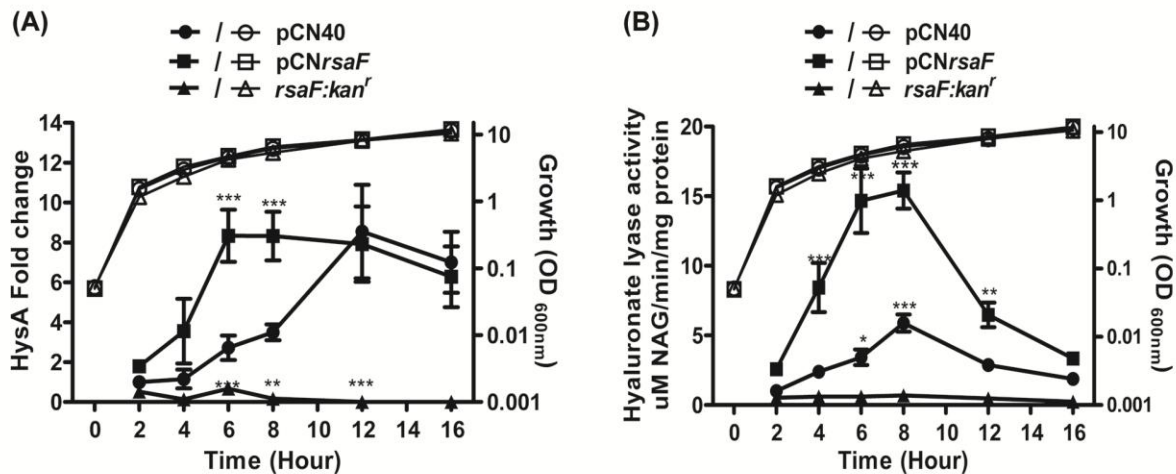


Figure 19: Influence of RsaF levels on the expression of HysA in *S. aureus* Newman.

(A) Time course measurement of *hysA* transcripts by qRT-PCR in control (pCN40), RsaF overexpression (pCNrsaF) and disruption (*rsaF::kan^r*) strains. Values were normalized against 5S rRNA and fold change in expression was determined by the standard $\Delta\Delta C_t$ method referred to the control at 2 hour of growth. (B) Hyaluronate lyase activity by spectrophotometric assay. Significant up regulation of (2-4 fold) *hysA* transcripts and hyaluronate lyase activity was revealed at 4 and 6 hour in RsaF overexpression. A marked reduction in *hysA* transcripts by 0.2-0.0002 fold and activity by 0.2-0.1 fold was seen in *rsaF* disruption strain. Experiments were performed in triplicate; mean and standard deviation are plotted. Filled symbols (●/■/▲) indicate the fold change in RsaF expression and open symbols (○/□/△) indicate the growth. * represents the statically significant difference analyzed by two-way ANOVA. *** (P<0.001), ** (P<0.01) and * (P<0.05).

As shown in Fig. 11 A, RsaF interacts with *hysA* mRNA *in silico* at 22-nucleotides spanning the 5' UTR, Shine-Dalgarno sequence and eight nucleotides at 5' coding region. Analyses by qRT-PCR and spectrophotometric assay resulted in a 2–4-fold increase in *hysA* transcript level (Figure 19A) as well as in hyaluronate lyase (HL) activity (Figure 19B) along growth, under RsaF overexpression. In comparison to the above, a significant down-regulation of *hysA* transcripts by 0.2–0.0002 and HL activity by 0.2–0.1 fold was observed in *rsaF* disruption strain (Figure 19A and B). These results on qRT-PCR and hyaluronate lyase activity support the positive regulation of *hysA* by the small RNA RsaF.

The increased activity of hyaluronate lyase results into loss of structural integrity and necrosis of the tissues, allowing pathogen access to deeper tissues (Hynes and Walton, 2000).

Hyaluronate lyase secreted by many gram positive pathogens have shown functions in biofilm and tissue invasion (Ibberson *et al.*, 2016). Hyaluronic acid present into the extracellular matrix serving as a structural component of *S. aureus* biofilm is degraded by HysA, providing a carbon source to the planktonic cells facilitating dissemination into the host (Ibberson *et al.*, 2016).

4.7.2 Influence of RsaF on biofilm formation

RsaF regulates the expression HysA which degrades hyaluronic acid, an important component of the biofilm matrix. The physiological influence of RsaF on biofilm formation, as assessed by both crystal violet-stained microtiter plate assay and confocal microscopy, proved its positive regulatory role on HysA. Cells were grown on BHI medium in the presence or absence of exogenous HA. Disruption of *rsaF* featured a 45% increase in the levels of biofilm compared to the control strain, in normal media (Figure 20) and further increased by 93% when supplemented with exogenous HA. Conversely, the overexpression of RsaF resulted in decreased levels of biofilm formation by 20% under normal growth medium, and by 27% when supplemented with external HA.

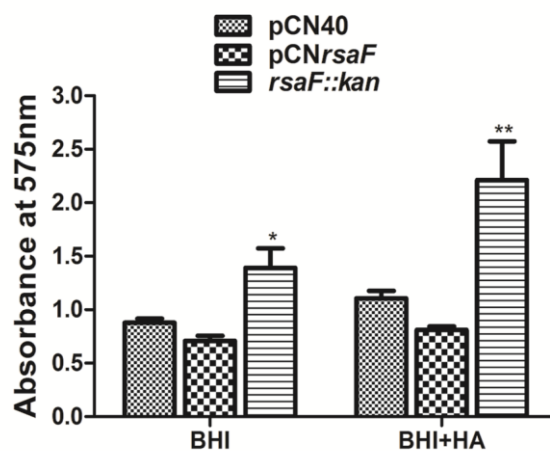


Figure 20: Influence of RsaF on biofilm formation.

Microtiter plate assay of biofilm in *S. aureus* Newman expressing altered levels of RsaF: control (pCN40), SprX1 overexpression (pCNrsaF) and disruption (*rsaF::kan*) constructs in presence and absence of HA. Statistical difference ($P \leq 0.0001$) between the constructs was determined by using one way ANOVA in comparison with the vector control.

Microscopically, there was no substantial difference in biofilm formation on the glass cover slip, under the influence of added HA for each RsaF⁺ strain. However the disruption strain demonstrated complex biofilm composed of tightly packed cells in presence of exogenous HA

(Figure 21). Overall, RsaF overexpression strain exhibited reduced biofilm formation compared to the control strain).

In vitro studies on biofilms showed the incorporation of exogenously supplied HA into the biofilm matrix which increases the biofilm biomass (Ibberson *et al.*, 2016). Disruption of RsaF resulted in *hysA* down regulation and in turn, increased biofilm formation in this study, which corroborates with the previous reports (Ibberson *et al.*, 2016) of increased biofilm formation observed in *hysA* mutant.

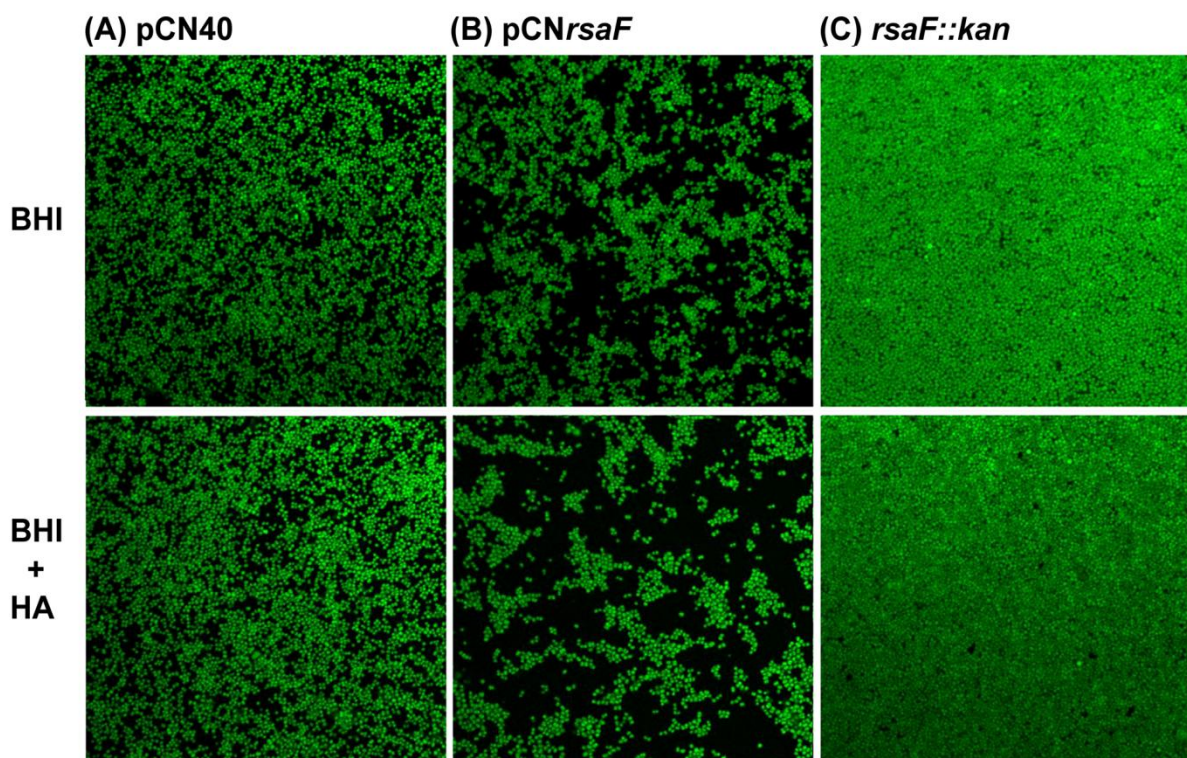


Figure 21: Fluorescence microscopy images of biofilms formed on the glass cover slip. Upper panel shows the biofilms formed in BHI medium supplemented with 0.2% glucose and lower panel illustrate the biofilms formed in presence of 0.2% glucose and HA (2 mg/ml). (A) control (pCN40), (B) RsaF overexpression (pCNrsaF) and (C) disruption (*rsaF::kan*) of *S. aureus* Newman, respectively.

The reduced activity of hyaluronate lyase exhibited by the *rsaF* mutant strain of *S. aureus* in our studies may turn the mutant strain hypo-virulent, as reduced HysA levels have shown negative effect on the degree of pathology as demonstrated by the size and number of viable bacteria recovered from skin lesion (Makris *et al.*, 2004). HysA has been characterized as a spreading factor of *S. aureus* and HysA mutant showed reduced severity in phenotype in models of acute pulmonary and cutaneous infection (Hart *et al.*, 2013; Ibberson *et al.*, 2014; Makris *et al.*, 2004).

4.8 RsaF positively influences the expression of serine protease like protein D (SplD) in *S. aureus* Newman

splD is encoded in an *spl* operon (a group of six serine proteases *splA-splF*) and have shown a protease activity targeting specific proteins involved in host-pathogen interaction (Paharik et al., 2017; Stentzel et al., 2017; Zdzalik et al., 2013). A time course measurement of *splD* mRNA levels by qRT-PCR under modified levels of RsaF revealed 0.8–0.005 fold reduction in *rsaF* disruption strain whereas RsaF over expression did not show any significant difference when compared with the control (Figure 22A).

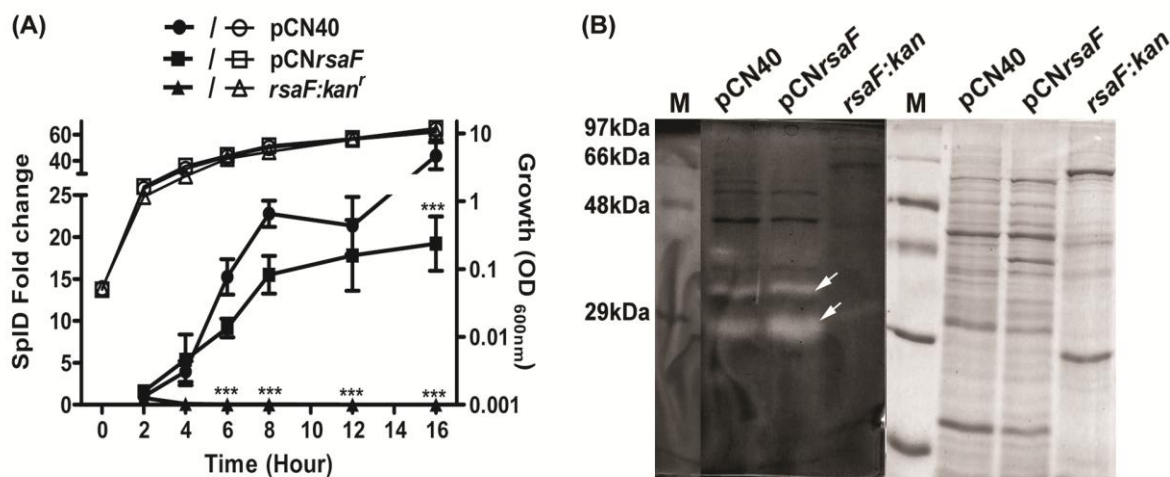


Figure 22: Expression of SplD under altered levels of RsaF.

(A) Time course qRT-PCR of *splD* transcripts in control (pCN40), overexpression (pCNrsaF) and disruption (*rsaF::kan^r*) strains. Values were normalized against 5S rRNA and fold change was calculated as per standard $\Delta\Delta C_t$ method referred to the control at 2 hour of growth. Filled symbols ($\bullet/\blacksquare/\blacktriangle$) indicate the fold change in RsaF expression and open symbols ($\circ/\square/\triangle$) indicate the growth. Significant down regulation of *splD* transcripts by 0.8-0.005 fold was revealed in *rsaF* disruption strain. Mean and standard deviation of triplicates are plotted. * represents the statically significant difference analyzed by two-way ANOVA. ***($P<0.001$). (B) Left: Zymography of total extracellular proteins, separated on PAGE containing 0.1% gelatin as a substrate. Inset arrows indicate proteases down regulated in *rsaF* disruption strain. Right: Coomassie blue stained loading controls.

The protease activity of the strains expressing altered levels of RsaF was analyzed by zymography at the stationary phase. Protease activity was visualized as a clear band against the stained gelatin background. Significant reduction in the over- all protease activity in the range of 43–22 kDa was observed in *rsaF* disruption strain (Figure 22B). An increase was seen in the case of *rsaF* over expression. The major down-regulation in the protease activity was found at the 21–23 kDa which corresponds to the serine proteases of *spl* operon and at around 33 kDa which indicates either a metalloprotease (Aur) or a serine protease SspA. The identity of the reduced proteases was interpreted from the previous reports (Reed et al., 2001; Shaw et al.,

2004). RsaF perhaps influenced the translation of SplD, since overexpression did not significantly change in *splD* mRNA levels but resulted in an increase in protease activity. SplD and other closely related proteases secreted by *S. aureus* have been identified as inducers of allergic asthma (Stentzel *et al.*, 2017). SplD without adjuvant elicited allergic lung inflammation characterized by Th2 cytokines and eosinophil infiltration. The higher titers of SplD-specific IgE in serum of asthmatic patients suggest the role of SplD in the pathogenesis of asthma (Stentzel *et al.*, 2017). SplD induces Th2-biased inflammatory response accompanied by the release of the innate cytokine IL-33. Stimulation of isolated epithelial cells with SplD *in vitro* have shown a direct effect of SplD on IL-33 production (Krysko *et al.*, 2019). The reduced expression of SplD transcripts seen under *rsaF* disruption indicates a positive influence on SplD by sRNA RsaF.

4.9 RsaF directly interacts with *hysA* and *splD* mRNAs

The potential interaction of sRNA RsaF to the *in silico* predicted targets *hysA* and *splD* mRNAs was investigated by an *in vitro* electrophoretic mobility shift experiment using *in vitro* transcribed and gel-purified RNA sequences of RsaF, *hysA* and *splD* corresponding to the predicted interaction regions.

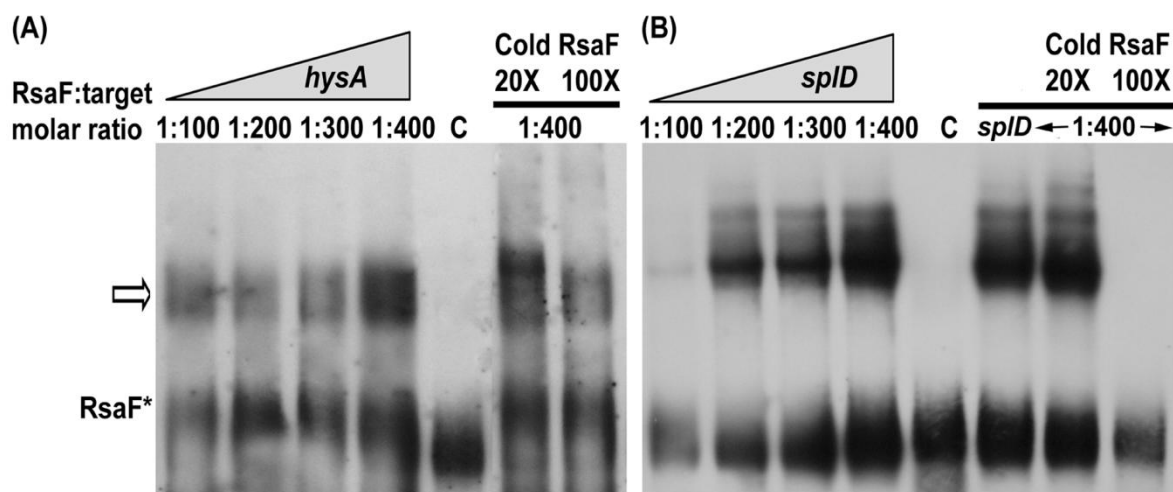


Figure 23: Interaction of RsaF with *hysA* and *splD* mRNAs by electrophoretic mobility shift assay.

DIG-labeled RsaF (0.01 pmol) incubated with unlabeled mRNAs in an increasing molar ratio (1, 2, 3, 4 pmol). Complex was resolved on 6% native-PAGE gel blotted and detected by anti-DIG antibody. (A) RsaF interaction with *hysA* mRNA. (B) Interaction of RsaF with *splD* mRNA. Labeled RsaF serve as a control. Specificity of the interaction was analyzed by cold RsaF.

Incubation of DIG-labeled RsaF with increasing molar ratio of *hysA* or *splD* transcripts resulted in a strong complex in the higher molecular weight range for RsaF-HysA and RsaF-SplD mRNA interactions (Figure 23A and B) at the maximum molar ratio (1:400) tested

(0.01 pmol of RsaF and 4 pmol of HysA / SplD). The specificity of the RsaF-HysA and RsaF-SplD mRNA interaction was demonstrated in the presence of 100x unlabeled RsaF that resulted in a decreased intensity or disappearance of the complex. The strong interaction of RsaF with *hysA* and *splD* mRNA *in vitro* imply that RsaF influences the expression of HysA and SplD by direct interaction with its mRNA. RsaF directly interacts with *splD* mRNA.

The strong complex of *hysA /splD* mRNA-RsaF observed in *in vitro* RNA-RNA interaction signifies the positive regulation of *hysA* and *splD* through a direct base pairing between RsaF and mRNA targets.

4.9.1 Influence of RsaF on *hysA/splD* mRNA stability

The stability and half lives of both *hysA* and *splD* mRNAs were tremendously reduced in the absence a functional RsaF. Following transcription inhibition by rifampicin, the *hysA* mRNA displayed a half-life of ~18 min in control, and was reduced to 1 min in *rsaF* disruption strain (Figure 24A). In a similar line, the *splD* mRNA half-life of ~10 min in the control was decreased to less than 1 min in the RsaF mutant (Figure 24B). Overexpression lead to 15 % - 18 % increases in mRNA levels and half life of 17 min for SplD, while it was less marked for HysA, with a half-life of 21 min (Figure 24).

Interaction with RsaF imparted stability to *hysA/splD* mRNAs thus positively influencing their expression. Several sRNAs involved in positive regulation employ an anti-antisense mechanism which involves unfolding of an intrinsic translation inhibitory structure, leading to accessibility of mRNA by ribosomes (Papenfort and Vanderpool, 2015). Examples for these are RNA III, involved in the regulation of *hla* mRNA encoding *S. aureus* α -toxin, (Morfeldt et al., 1995) and Qrr in *V. cholerae*, influencing *vca0939* mRNA which is involved in cyclic-di-GMP synthesis (Zhao et al., 2013). In another mechanism, sRNA base pairs prevent interference with ribonucleolytic decay, mediated by RNases that contributes to RNA processing or degradation, Such interference has been reported for FasX sRNA of *Streptococcus* which base pairs at the 5'UTR of *ska* mRNA, encoding streptokinase, to prevent RNase E-mediated degradation (Ramirez-Peña et al., 2010). The major RNases found in *S. aureus* are RNase III (ds-RNA endonuclease), RNase-Y (ss-RNA endonuclease), RNaseJ1/J2, RNaseP (Bonnin and Bouloc, 2015). Yet the exact molecular mechanism of activation, for many sRNA-target interactions in *S. aureus*, such as in the cases of regulation of target virulence genes by sRNAs Teg49 (Manna et al., 2018), Teg41 (Zapf et al., 2019), SprX (Kathirvel et al., 2016) etc. is not dissected. The strong complex of *hysA/splD* mRNA-RsaF observed in *in*

in vitro RNA-RNA interaction signifies the positive regulation of *hysA* and *splD* through a direct base pairing between RsaF and mRNA targets.

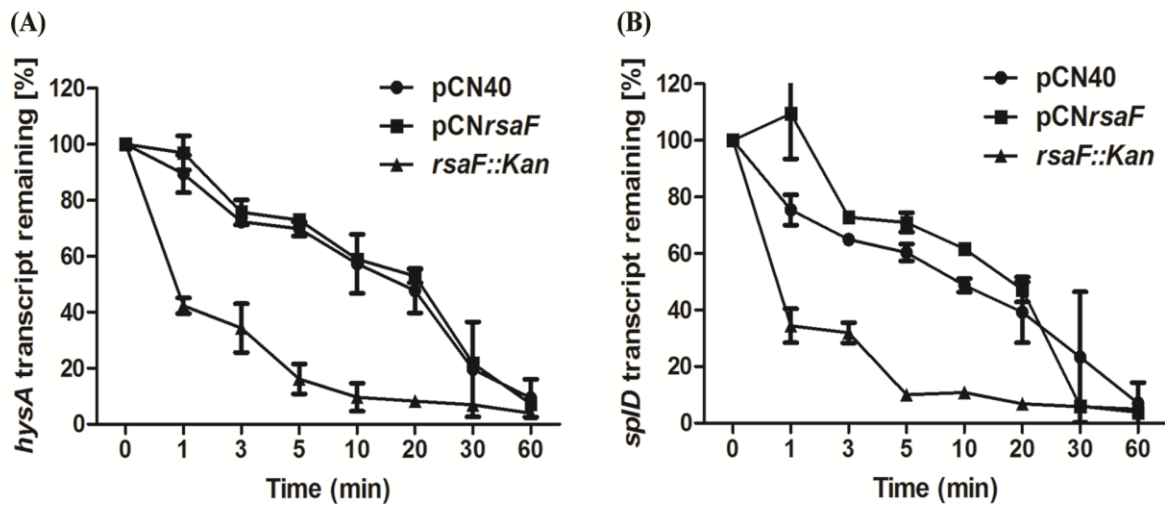


Figure 24: Half-life determination of *hysA* / *splD* mRNA in *S. aureus* strains.

mRNA Half-life measured in control (pCN40), overexpression (pCNrsaF) and disruption (*rsaF::kan'*) strains. (A) Half-life of *hysA* mRNA in the control strain revealed about ~20 min and reduced to 1 min in *rsaF* disruption strain (B) Half-life of *splD* mRNA in control strain is about ~10 min and reduced to less than 1 min in *rsaF* disruption mutant. Values were normalized against 5S rRNA and fold change was calculated as per standard $\Delta\Delta C_t$ method referred to the control at 0 min.

The increased mRNA stability by RsaF seen in this study is possibly the result of formation *hysA* / *splD* mRNA-sRNA duplex that either caused an enhanced ribosome accessibility and translation rate, or, prevented the mRNA from degradation by RNases. The interaction RsaF at the 5'UTR (-22 to +8), inclusive of ribosome binding site (RBS) of *hysA* favors the notion of an antisense mechanism facilitating the unfolding of a translation inhibitory structure, which was indicated in the *in silico* minimal energy secondary structure, predicted for *hysA* mRNA. The interaction sequence of *splD* mRNA is located ~30 nt upstream the RBS within the inter-cistronic space between *splC* and *splD*.

4.10 Regulatory network of HysA and SplD

In silico analysis has shown RsaF to base pair at the 5' UTR of *hysA* mRNA and *splD* mRNA. Expression of *hysA* is reported to be positively regulated by Agr and negatively regulated by SarA at the exponential growth phase (Hart et al., 2013; Makris et al., 2004; Oriol et al., 2021). A metabolic regulator CodY acts as a repressor of *hysA* expression which establishes a link between metabolism and virulence (Brinsmade et al., 2010; Ibberson et al., 2014). CodY negatively regulates *agr* system and in turn some *hysA* regulation occurs through CodY-*agr* interactions (Roux et al., 2014). This study revealed an increase in the *hysA* expression and its activity in the presence of enhanced levels of RsaF. Conversely, the significant reduction of

hysA expression in RsaF disruption strain indicates the role of RsaF in regulation of hyaluronate lyase expression in *S. aureus* Newman.

This study also reveals SplD as the target regulated by small RNA RsaF. The expression of *splD* is positively regulated by the global accessory gene regulator (*agr*) and negatively regulated by Repressor of toxin (Rot) (Saïd-Salim et al., 2003) and CodY (Gimza et al., 2019). In this study, disruption of *rsaF* showed a strong down regulation of *SplD* expression whereas overexpression did not show any significant difference. Total protease activity when analyzed by zymography also showed a reduced expression of proteases in case of RsaF disruption.

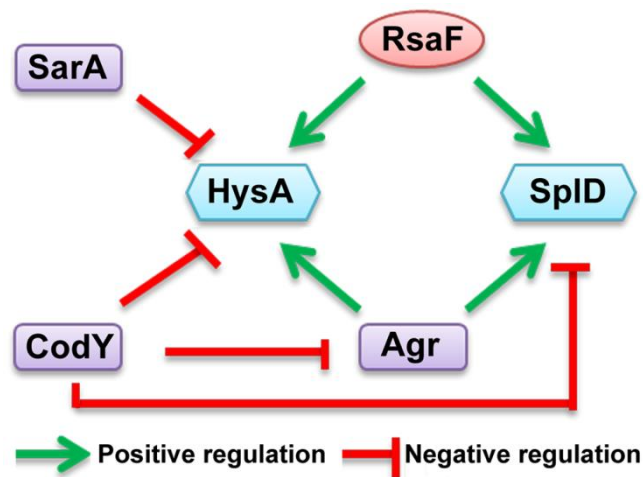


Figure 25: Complex and multi-factorial regulatory network of Hyaluronate lyase and SplD regulation in *S. aureus*.

Our results suggest that RsaF adds an additional layer of regulation that influences the expression of potent virulence factors hyaluronate lyase and serine protease like protein D. The *in vitro* RNA-RNA interaction indicates the positive regulation is through a direct base pairing between RsaF and *hysA/splD* mRNA.

These observations on the role of RsaF on HysA and SplD regulation give insight into the combined regulation and fine tuning of these virulence determinants by multiple regulators during infection by *S. aureus* (Figure 25).

4.11 Significance of sRNA RsaF in *S. aureus* Newman

S. aureus is a versatile human pathogen and this versatility is attributed to the arsenal of virulence factors. These factors activate virulence and metabolic pathways of bacteria to ensure its survival against the host immune system. *S. aureus* has numerous regulators that, alone and in combination, control the expression of these virulence factors. Small RNAs, emerging as regulators, enable bacterial pathogens to express virulence genes when required during infections, illustrating their crucial roles in pathogenesis.

Small RNAs RsaA (Romilly et al., 2014; Tomasini et al., 2017), RsaC (Lalaouna et al., 2019), RsaD (Augagneur et al., 2020), and RsaE (Bohn et al., 2010) from the group of 11 novel small RNAs (RsaA-K) identified by Geissmann *et al.* (2009) have shown significant impact on virulence by modulating the expression levels of target mRNAs through various networks.

RsaA represses the synthesis of MgrA and regulates peptidoglycan metabolism, biofilm formation, and favors chronic infections (Romilly et al., 2014; Tomasini et al., 2017). RsaC favors the oxidative stress response (Lalaouna et al., 2019), RsaD regulates carbon metabolism (Augagneur et al., 2020), and RsaE regulates the biofilm formation (Bohn et al., 2010). The small RNA RsaF was characterized for the first time in this study for its functional mechanism and significance, in the involvement of regulation of pathogenicity genes *hysA* and *splD* in the clinical isolate *S. aureus* Newman. The identification of hyaluronate lyase (HysA) and serine protease like protein D (SplD) as targets of RsaF by *in silico* analysis and the subsequent observation of their up-regulation by RsaF in real-time PCRs and physiological assays have determined the functional significance of this sRNA.

Hyaluronate lyase secreted by *S. aureus*, which breaks hyaluronic is known as the spreading factor of the infection and have shown functions in biofilm and tissue invasion (Ibberson *et al.*, 2016). RsaF, is also involved in regulation of biofilm formation in addition to already reported sRNAs, SprX1 (Kathirvel *et al.*, 2016), RsaA (Romilly *et al.*, 2014) and RNAlII (Chambers and Sauer, 2013) in *S. aureus*. An increase in the transcript levels of *hysA* and its activity in the presence of enhanced levels of RsaF and the significant reduction in RsaF disruption strain indicate the role of RsaF in modulation of hyaluronate lyase expression in *S. aureus* Newman.

Proteases are one of the major factors involved in invasion and colonization of *S. aureus*. Serine protease like protein D (SplD) encoded in an *spl* operon (a group of six serine proteases *splA-splF*) secreted by *S. aureus* have been identified as inducers of allergic asthma and has the more target specificity than SplA and SplB (Singh and Phukan, 2019; Stentzel et al., 2017). The reduced expression of SplD transcripts seen under *rsaF* disruption indicates a positive influence on SplD by sRNA RsaF. Total protease activity when analyzed by zymography also showed reduced expression of proteases under RsaF disruption.

In conclusion, the current study uncovers a novel role for the small RNA RsaF in fine regulation of secreted virulence factors hyaluronate lyase and Serine protease like protein D in *S. aureus* Newman.